Pulse-like ruptures induced by low-velocity fault zones

Yihe Huang[1] and Jean-Paul Ampuero[1]

[1]   Low-velocity fault zones (LVFZs) are found in most mature faults. They are usually 100–400 m wide and have ∼20%–60% wave velocity reductions relative to the country rock. To study the effect of LVFZs on earthquake rupture and the radiated wavefield, we conducted two-dimensional (2-D) simulations of dynamic rupture on faults that bisect a LVFZ, considering a range of velocity reductions and widths. Most earthquakes apparently have slip rise times much shorter than their overall rupture duration. A number of dynamic mechanisms for such pulse-like ruptures have been proposed, including frictional self-healing, fault strength heterogeneities, and bimaterial effects. We find that ruptures in LVFZs with strong enough wave velocity contrast behave as pulses. These pulses are generated by fault locking induced by waves reflected from the boundaries of the LVFZ. This mechanism of pulse generation is robust to variations of initial stress, smoothness of the LVFZ structure, rupture mode, and exclusion of frictional healing. Moreover, we find that LVFZs can generate complex rupture patterns. LVFZs with low-velocity reduction induce multiple rupture fronts involving coexisting pulses and cracks. LVFZs with certain widths can accelerate the transition to supershear rupture speed. These additional effects of LVFZs on dynamic rupture can contribute to the complexity of high-frequency ground motions.

1.   Introduction

[2]   Faults are usually surrounded by damaged rocks that are more compliant and have lower seismic wave velocities than the country rocks. The properties of such low-velocity fault zones (LVFZs) have been widely studied in different areas such as the San Andreas [*Li and Leary*, 1990; *Li et al.*, 2006; *Lewis and Ben-Zion*, 2010], San Jacinto [*Lewis et al.*, 2005; *Yang and Zhu*, 2010], Landers [*Li et al.*, 1994; *Peng et al.*, 2003; *Li et al.*, 2007], Hector Mine [*Li et al.*, 2002], Calico [*Cochran et al.*, 2009; *Yang et al.*, 2011], Nojima [*Mizuno et al.*, 2008], and North Anatolian [*Ben-Zion et al.*, 2003] fault zones. Travel times and waveform attributes of fault zone trapped waves and head waves can be exploited to determine the seismic wave velocity reduction and the width of the LVFZ, although there are trade-offs between these two properties. LVFZs usually have a width of 100–400 m (e.g., ∼200 m in the San Andreas fault, ∼300 m in the Landers fault), although some are much wider (e.g., ∼1.5 km in the Calico fault). The velocity reductions within the LVFZ, relative to the country rock, vary in the range of 20%–60%. The borehole data of the SAFOD drilling project reveals similar fault zone structures, with a ∼200 m LVFZ

and velocity reduction of ∼25% at the depth of ∼3.2 km [*Hickman et al.*, 2005]. The Hirabayashi borehole across the Nojima fault also shows a velocity reduction of ∼40% for *P* waves and ∼60% for *S* waves at a depth of ∼630 m (Figure 1).

[3]   In kinematic source models inferred from seismological and geodetic data, the rise time, i.e., the duration of slip at a given fault location, is generally much shorter than the whole earthquake duration and than the wave travel time across the seismogenic thickness [*Heaton*, 1990; *Beroza and Mikumo*, 1996]. This is in contrast to the long rise times produced by classical crack models of earthquake dynamics, like those that assume slip-weakening friction and homogeneous media [*Andrews*, 1976]. Many mechanisms for the generation of short-duration slip pulses are known: self-healing under velocity-dependent friction [*Perrin et al.*, 1995; *Beeler and Tullis*, 1996, *Zheng and Rice*, 1998], the generation of healing phases by heterogeneities of strength or initial stress on the fault [*Beroza and Mikumo*, 1996; *Oglesby and Day*, 2002; *Aagaard and Heaton*, 2008] or by the boundaries of the seismogenic fault region [*Day*, 1982a], and dynamic changes of normal stress induced by bimaterial effects [*Andrews and Ben-Zion*, 1997; *Cochard and Rice*, 2000; *Shi and Ben-Zion*, 2006; *Rubin and Ampuero*, 2007; *Ampuero and Ben-Zion*, 2008].

[4]   When an earthquake breaks in a fault embedded in a LVFZ, the trapped waves can alter the shear stress on the fault plane and affect the dynamic rupture process. *Harris and Day* [1997] studied dynamic ruptures on planar faults

---

[1]Division of Geological and Planetary Sciences, California Institute of Technology, Pasadena, California, USA.
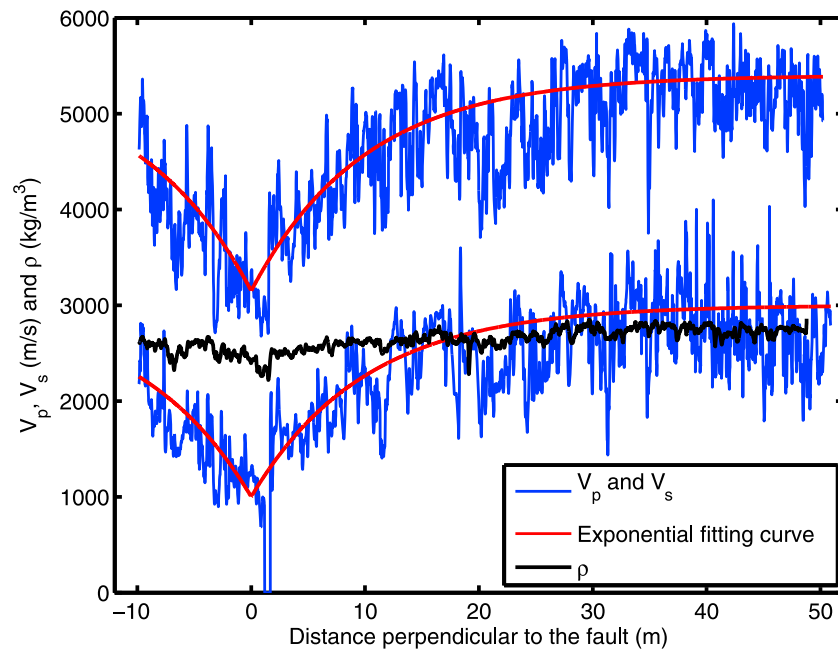
Figure 1. *P* wave speed, *S* wave speed, and density from a log in the Hirabayashi borehole crossing the Nojima fault zone, Japan, at about 630 m depth (data courtesy of Hisao Ito). The red curves are exponential distributions.

that bisect 100 to 4000 m wide LVFZs with 17% and 33% velocity reductions relative to the country rock. In their simulations, based on slip-weakening friction, the arrival of waves reflected from the edge of the LVFZ produced a complex pattern of slip rate. Others have studied earthquake nucleation, dynamic rupture, and earthquake cycles on LVFZs [*Ampuero et al.*, 2002; *Ben-Zion and Huang*, 2002; *Brietzke and Ben-Zion*, 2006; *Kaneko et al.*, 2011]. None of these previous studies found the LVFZ to induce slip pulses, except when bimaterial effects were at play.

[5] An extremely compliant LVFZ is equivalent to an elastic slab of finite thickness with fixed displacement boundary conditions. In such a configuration, analytical solutions of steady state rupture have exponentially decaying slip rates behind the rupture front, behaving practically like pulses [*Broberg*, 1999]. This conceptual end-member case suggests that a highly damaged LVFZ (perhaps more than in previous studies) might favor pulse-like rupture. Given the existence of a LVFZ in most mature faults, it seems natural to further investigate if it can contribute to short rise times. Here we performed dynamic simulations of two-dimensional (2-D) in-plane rupture on slip-weakening faults that bisect a LVFZ. Our model assumptions and methods are described in section 2. We show, in section 3, that the reflected waves in a LVFZ with low enough velocities indeed provide an efficient mechanism for the generation of pulse-like ruptures. We further analyze the influence of the velocity reduction and width of the LVFZ on the rupture process. We also show the robustness of our findings with respect to variations in the model, namely the effects of the initial stress, the smoothness of the velocity distribution within the LVFZ, mode 3 rupture, and frictional healing. In section 4, we discuss the properties

of slip pulses in a LVFZ and their potential effects on ground motions.

2. Model Setup

[6] We consider a planar fault that bisects a LVFZ of finite width W embedded in an infinite medium (Figure 2). We consider this symmetric problem to avoid the interference between two mechanisms that can generate short rise times: dynamic changes of normal stress in asymmetric configurations [*Harris and Day*, 1997; *Ben-Zion and Huang*, 2002; *Brietzke and Ben-Zion*, 2006] and unloading shear stresses from reflected waves. Our paper focuses on the latter mechanism. Both the LVFZ and the country rock are linear elastic isotropic materials. We performed simulations with different wave velocity reductions inside the LVFZ while assuming uniform density and Poisson's ratio. We define the relative velocity reduction as $\Delta v = 1 - v_{LVFZ}/v_{country}$.
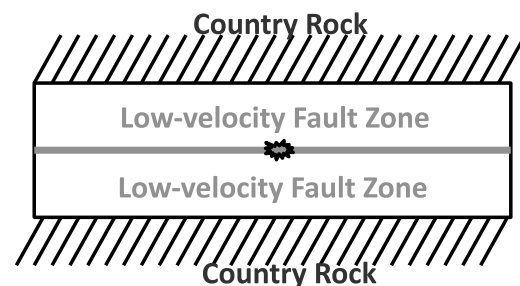

Figure 2. Model setup of 2-D dynamic rupture on a fault bisecting a low-velocity fault zone (LVFZ).
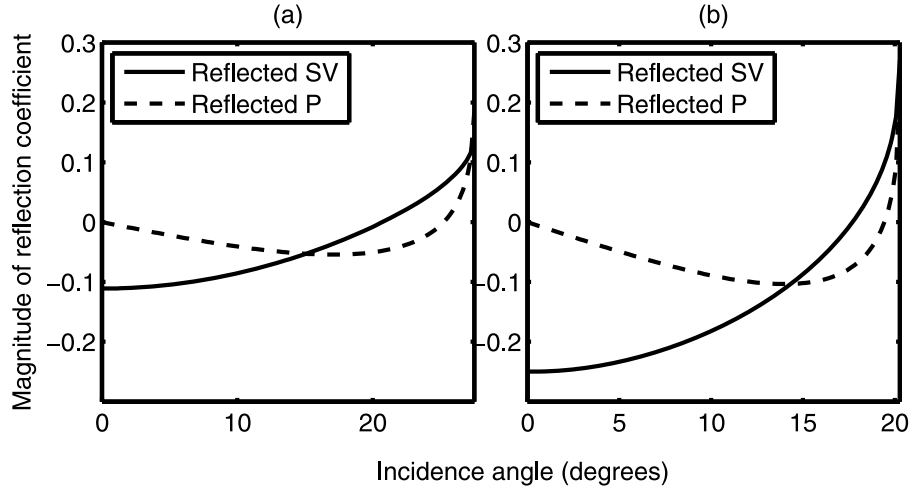
Figure 3. Reflection coefficients for incident *SV* waves at the boundary between country rock and LVFZs with velocity reductions of (a) 20% and (b) 40%, respectively, as a function of incidence angle. Incidence is from the LVFZ. Both *P* and *SV* reflected waves are considered. The incident angles of *SV* waves are plotted below the first critical angle. The phase is zero for this range of incident angles. Formulas of reflection coefficients are taken from *Aki and Richards* [2002].

[7] We assume a modified slip-weakening friction law, which combines linear slip-weakening friction and instantaneous healing, in order to exclude the mechanism of pulse generation that operates under more realistic velocity-dependent friction laws, even without a LVFZ [*Perrin et al.*, 1995; *Beeler and Tullis*, 1996; *Zheng and Rice*, 1998]. In the linear slip-weakening friction law [*Andrews*, 1976], the friction coefficient μ is a function of cumulative slip *D*:

$$\mu = \max\{\mu_d, \mu_s - (\mu_s - \mu_d)D/D_c\}, \tag{1}$$

where μ_d is the dynamic friction coefficient, μ_s is the static friction coefficient, and D_c is the critical slip. The static and dynamic friction coefficients in our simulations are 0.6 and 0.1, respectively. This low value of dynamic friction is consistent with the lack of heat flux anomaly on the San Andreas fault [*Kanamori and Heaton*, 2000; *Boullier et al.*, 2001; *Kano et al.*, 2006]. In our assumed instantaneous healing mechanism, the friction coefficient is locally reset to its initial value as soon as slip stops (in practice, if the slip rate becomes smaller than a very small value). We discuss in section 3.7 how the results differ if the fault remains at the dynamic strength level.

[8] We artificially initiate ruptures by imposing a time-weakening nucleation zone that expands at constant speed [*Andrews*, 1985], one quarter of the *S* wave speed of the country rock. The rupture starts propagating spontaneously when it reaches a certain critical size. Shortly after, the nucleation procedure is removed and the friction coefficient is allowed to heal. The prescribed nucleation speed is slow enough to avoid abrupt perturbations on dynamic rupture and fast enough to allow efficient computations. Selected simulations with much slower nucleation produced similar results during spontaneous rupture growth. Simulations initiated by an overstressed region, a more abrupt nucleation procedure, produced short rise times more systematically, reinforcing our main result described in section 3. For a given initial shear stress, we found the critical size for spontaneous rupture to be rather independent of the LVFZ width. Indeed, for the relatively low initial stress levels and narrow LVFZs considered here, the critical size is expected to be more sensitive to the country rock.

[9] We solve the dynamic rupture problem in 2-D plane strain (Figure 2) using a spectral element method (SEM2DPACK, http://www.sourceforge.net/projects/sem2d/). We verified the code on a 2-D version of the SCEC TPV3 benchmark problem [*Harris et al.*, 2009]. We found that the SEM has the same convergence rate as the DFM [*Day*, 1982b; *Rojas et al.*, 2008]. We also verified the numerical convergence of the SEM in problems involving a LVFZ. We discuss the benchmark and convergence tests in the appendices. In all the simulations reported here, we set, by trial and error, a spectral element size small enough to sample the process zone with more than three Gauss-Lobatto-Legendre nodes.

[10] In order to apply our results to a wide range of material properties, we adopt dimensionless quantities for slip, space, time, slip rate, and stress:

$$D^* = D/D_c, \tag{2}$$

$$x^* = x/L_c, \tag{3}$$

$$t^* = tv_s/L_c, \tag{4}$$

$$V^* = VL_c/D_c v_s, \tag{5}$$

$$\sigma^* = \sigma/\Delta\tau_s, \tag{6}$$

where $\Delta\tau_s = \sigma_0(\mu_s - \mu_d)$, $L_c = GD_c/\Delta\tau_s$, *G* is shear modulus, and v_s is *S* wave velocity. The normalized density, critical slip, and shear modulus are all 1. As a result, the normalized *S* wave speed and *P* wave speed are 1 and 1.732, respectively. The normalized normal stress is 2.
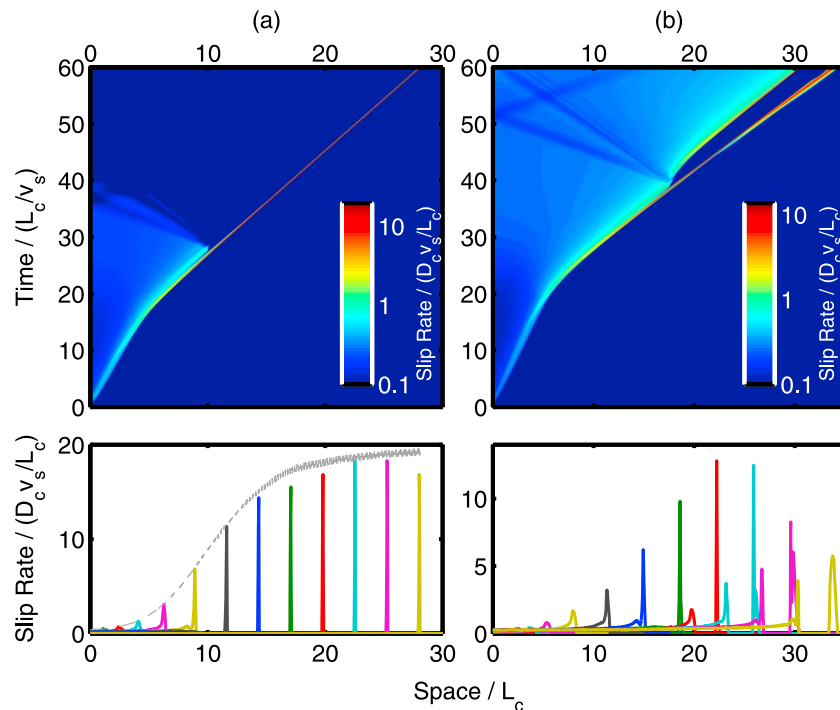
Figure 4. Spatiotemporal distributions of slip rate and its spatial distributions at time intervals of 5 for LVFZs of width 1 with velocity reductions of (a) 40% and (b) 20%. In both simulations the S ratio is 2.33.

We quantify the initial stress level by the nondimensional relative strength parameter S defined by *Das and Aki* [1977] as the ratio of initial strength excess to stress drop: $S = (\mu_s - \mu_0)/(\mu_0 - \mu_d)$.

3. Results

3.1. Low-Velocity Fault Zones Can Induce Pulse-Like Ruptures

[11] The amplitude of a wave reflected back to the fault from the boundary of a LVFZ has a sign opposite to that of the incident wave for a certain range of incidence angles (Figure 3). Thus, it is conceivable that under certain conditions the reflected wave can unload the fault and heal the rupture, generating a slip pulse. Figure 4a shows the spatial-temporal distribution of the slip rate in a simulation with $W = 1$ and $S = 2.33$. The rupture starts as a crack, which is the expected behavior for slip-weakening models in homogeneous media. However, at a certain distance, a back-propagating healing front emerges spontaneously. This feature is similar to the stopping phase that would arise from the abrupt arrest of a crack, but we note that the simulation does not contain any stopping barrier. Subsequently, the rupture transforms into a pulse and continues propagating. The pulse soon reaches steady state. Its rise time (∼0.3) is comparable to the travel time of P and S waves across the LVFZ. Its rupture speed is close to the Rayleigh wave speed of the LVFZ. The peak slip rate increases during the initial crack-like propagation and becomes stable once the rupture becomes a steady state pulse.

[12] In the following sections we assess the robustness of the pulse generation mechanism, illustrated by this example, by exploring how the rupture style is affected by the wave speed in the LVFZ, the width of the LVFZ, and the initial stress. The main effects on rupture speed and style are summarized in Figure 6. We further consider variations about the basic model, including a smoother distribution of wave speed in the LVFZ, rupture in mode 3, and exclusion of frictional healing.

3.2. Effect of the Velocity Reduction in the LVFZ

[13] The velocity reduction in natural LVFZs typically ranges from 20% to 60%. We conducted simulations with a range of velocity reductions ($\Delta v = 0.2, 0.3, 0.4,$ and 0.5) and found pulses in all cases. The pulse emerges sooner in LVFZs with larger Δv, as expected from their larger reflection coefficients inducing unloading reflected waves of higher amplitude (Figure 3). We found, however, distinct rupture styles and speeds at high and low Δv. For $\Delta v = 0.4$ and 0.5, ruptures eventually propagate as pure pulses (Figure 4a) with speeds approaching the Rayleigh wave speed of the LVFZ material (hereafter called "LVFZ Rayleigh"). Their short rise time (∼0.3 for $\Delta v = 0.4$ and ∼0.35 for $\Delta v = 0.5$) is comparable to the wave travel time across the LVFZ. Slip and slip rate are larger in the case with higher wave speed reduction. For $\Delta v = 0.2$ and 0.3, ruptures feature a pulse followed by a crack (Figure 4b). Their rupture speed eventually approaches the Rayleigh speed of the country rock (hereafter called "country Rayleigh"). The peak slip rate increases during the initial crack-like propagation but decreases to a much lower level after the onset of the country Rayleigh pulses. While these pulses are super-shear with respect to the LVFZ material, they are not generated by the Burridge-Andrews mechanism, which requires high initial shear stress [*Andrews*, 1976], but by the multiple reflected waves from the boundary of the LVFZ. Their rise
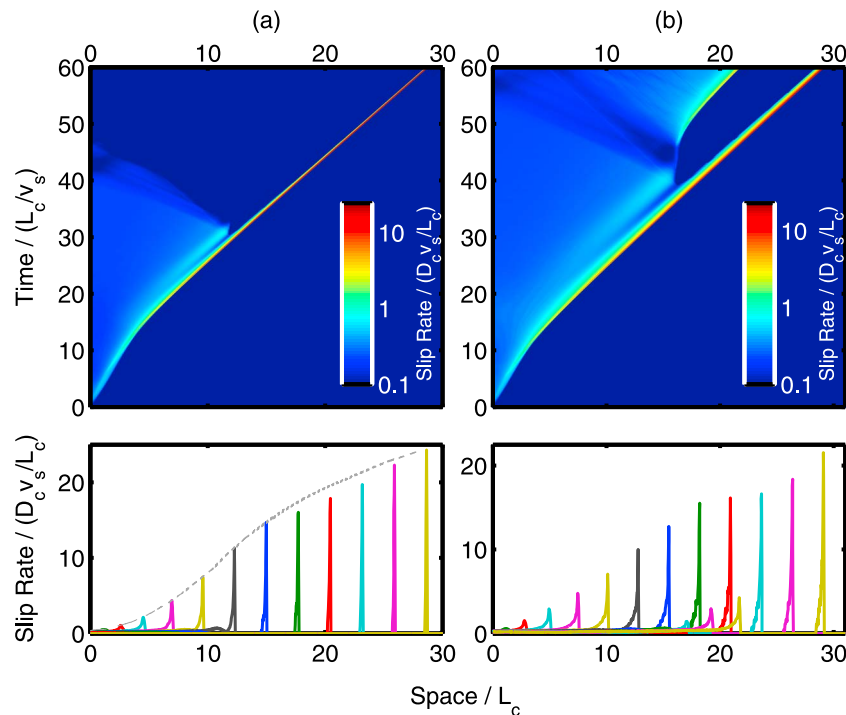
Figure 5. Slip rate (same representation as in Figure 4) for S ratio of 2.33 and LVFZs with velocity reduction of 40%. The LVFZ widths are (a) 2 and (b) 4.

times (~1.5 for $\Delta v = 0.2$ and ~2 for $\Delta v = 0.3$) are much longer than those of the LVFZ Rayleigh pulses.

3.3. Effect of the LVFZ Width

[14] We explored the effect of the LVFZ width by varying W from 1 to 4, while keeping all the other parameters the same as in our previous simulations. For a LVFZ of $\Delta v = 0.4$, the rupture speed stays at LVFZ Rayleigh level, while the rupture style changes. When $W = 1$ and 2, the rupture starts as a crack and later transforms into a LVFZ Rayleigh pulse (Figures 4a and 5a). When $W = 4$, pulses and cracks coexist simultaneously: the pulse is followed by a crack (Figure 5b). For wider LVFZs, the onset of pulse-like rupture happens later; the pulses reach steady state later and their rise time at steady state is roughly proportional to W. These observations are consistent with the proportionality between W and the travel time of the fault zone reflected waves. Figure 6a summarizes the effects of the velocity and width of LVFZs on the rupture style and rupture speed.

3.4. Effect of Initial Stress and LVFZ Width on Rupture Speed

[15] In a 2-D homogeneous medium, ruptures can run at supershear speed only if $S < 1.77$ [*Andrews*, 1985]. As expected, when $S = 2.33$ we observed only subshear ruptures, LVFZ Rayleigh or country Rayleigh. When $S = 1.67$ we observe a range of rupture speeds on LVFZs with $\Delta v = 0.2$ (Figure 6b). When $W = 1$ the rupture runs faster than the S wave speed of the LVFZ, approaching the country Rayleigh speed (Figure 7a). When $W = 2$ the rupture undergoes the transition from LVFZ Rayleigh to supershear speed relative to the country rock, faster than the P wave of the LVFZ (hereafter called "country supershear"). When $W = 4$ the

rupture speed approaches the P wave speed of the LVFZ (hereafter called "LVFZ supershear"). When $W = 8$ (not shown here) the rupture speed is near the LVFZ Rayleigh. The distance at which the supershear transition would happen in a homogeneous medium when $S = 1.67$ is much larger than the size of our simulation domain. Hence, for a certain range of LVFZ widths we find that the presence of the LVFZ allows the supershear transition to happen sooner than expected. This phenomenon is also present in the simulations of *Harris and Day* [1997]. We observe similar effects when $\Delta v = 0.4$ (Figure 6c). In addition, LVFZs of $\Delta v = 0.4$ still favor pure pulse-like rupture for $W = 1$ (Figure 7b) and 2. When $S = 1$ the supershear transition happens very early and the effect of the LVFZ is less marked. *Biegel et al.* [2008] also found a dependence of rupture speed on the damaged zone width in laboratory experiments, with a transition from country Rayleigh to LVFZ Rayleigh as a function of W. Some of their experiments ran significantly slower than the LVFZ Rayleigh speed, which they attributed to anelastic dissipation in the damaged zone, a mechanism ignored in our simulations.

3.5. Effect of the Smoothness of the LVFZ Structure

[16] Wave velocities do not necessarily change abruptly inside natural LVFZs but rather decrease progressively, as exemplified by the Nojima fault zone seismic log (Figure 1). A smoother LVFZ structure is expected to be less efficient at reflecting and trapping waves than a LVFZ with abrupt velocity contrasts. To assess how the smoothness of the LVFZ structure competes with the pulse generation mechanism, we consider a LVFZ with an exponential distribution of wave speeds as a function of distance z to the fault plane: $v(z) = v_0(1 - \Delta v \exp(-5z/W))$, where v_0 is the country rock
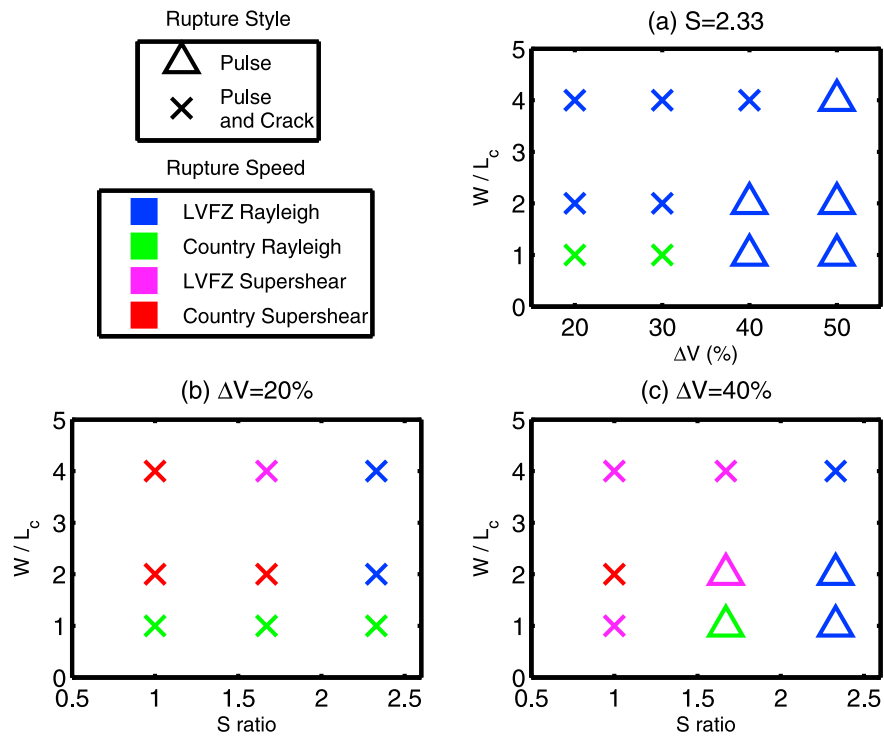
Figure 6. Summary of rupture style and rupture speed (a) as a function of velocity reduction and LVFZ width for an S ratio of 2.33 and as a function of S ratio and LVFZ width for velocity reductions of (b) 20% and (c) 40%.

velocity, Δv is the relative velocity change, and W is the width of the zone where more than 92% of the total velocity reduction is achieved, i.e., $(v(W/2) - v(0))/v_0 \sim 0.92\Delta v$. We found that simulations with $W = 1$ and $\Delta v = 0.4, 0.5,$ and 0.6 can still produce pulses. Their rupture speed increases as Δv decreases and remains higher than the lowest S wave speed inside the LVFZ but lower than the country Rayleigh speed. As Δv increases, the ruptures behave more pulse-like than
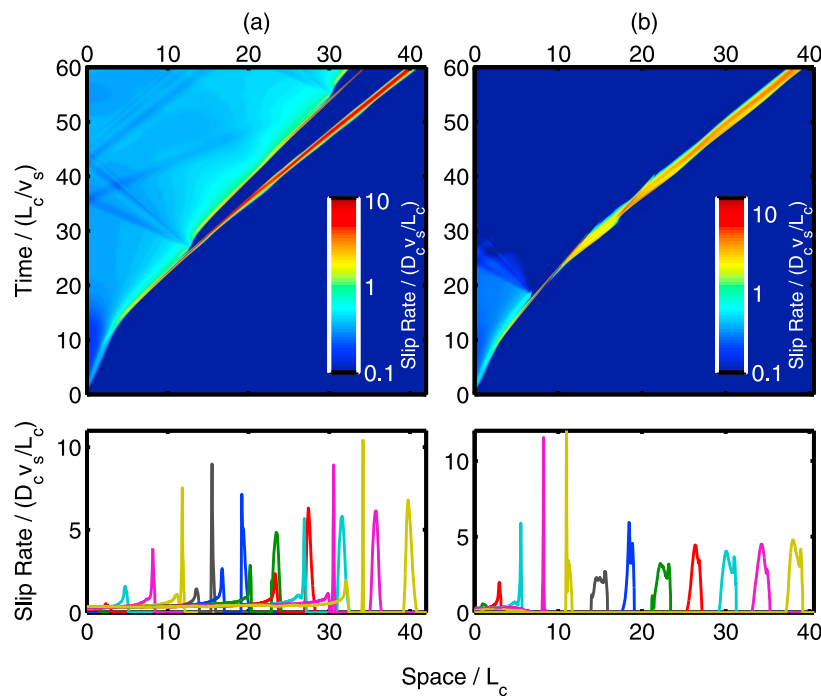

Figure 7. Slip rate (same representation as in Figure 4) for an S ratio of 1.67 and LVFZs of width 1 with velocity reductions of (a) 20% and (b) 40%.
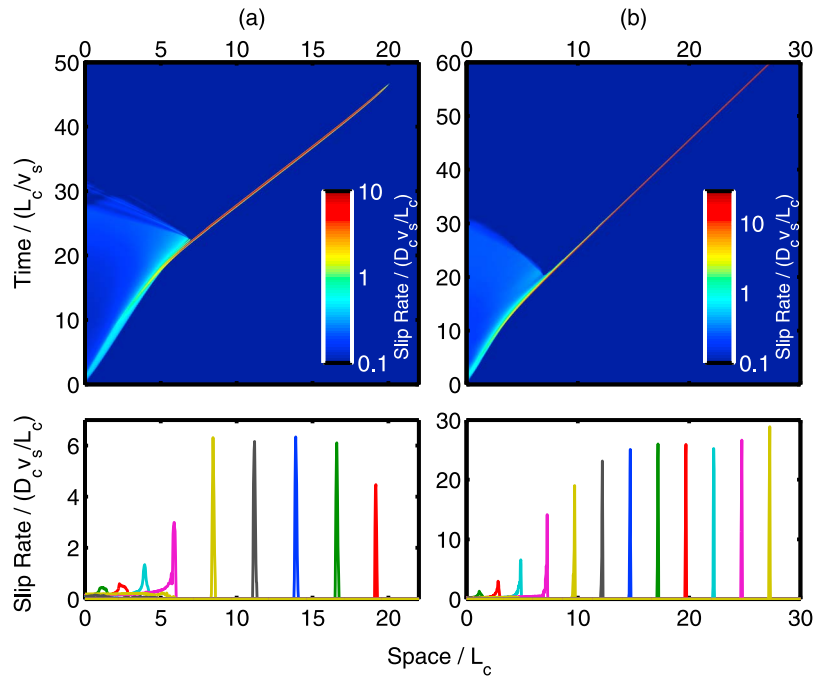
Figure 8. (a) Slip rate (same representation as in Figure 4) for an S ratio of 2.33 and LVFZ with exponential distribution of wave speeds in the in-plane mode. The LVFZ is 1 wide with a maximum velocity reduction of 60%. (b) Slip rate (same representation as in Figure 4) for an S ratio of 2.33 and LVFZ of width 1 with a velocity reduction of 50% in the antiplane mode.

crack-like. For $\Delta v = 0.6$ (Figure 8a), a pure pulse with an average rise time of ~0.5 eventually emerges, leaving a dying crack behind. Interestingly, after some propagation distance the pulse stops spontaneously.

3.6. Effect of the Rupture Mode

[17] Our study considered so far the in-plane rupture mode (mode 2), relevant to along-strike rupture propagation on strike-slip faults or to along-dip propagation on dip-slip
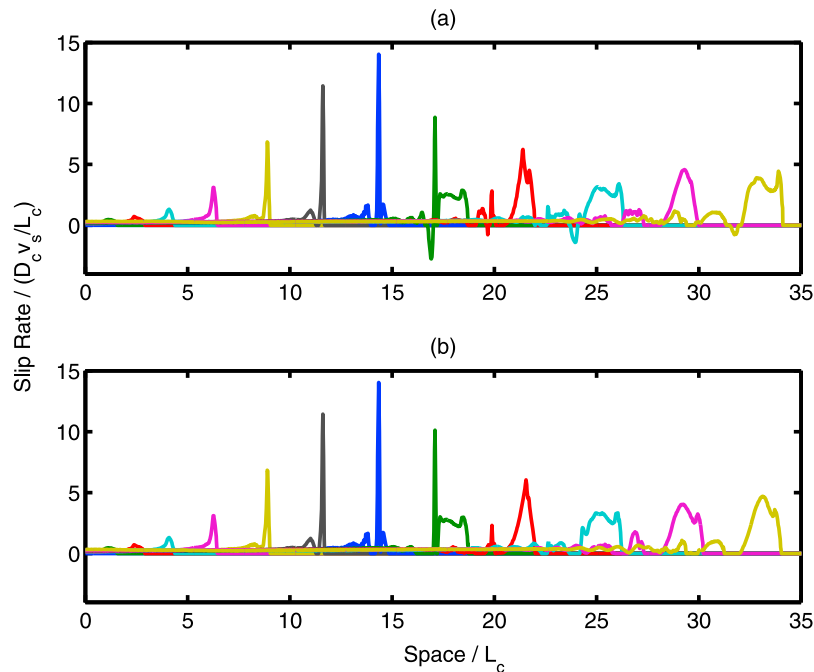

Figure 9. Spatial distributions of slip rate at time intervals of 5 for an S ratio of 2.33 and LVFZs of width 1 with a velocity reduction of 40%. The dynamic friction coefficients are (a) 0.1 and (b) 0.3, respectively. Both simulations are without frictional healing.

faults. We found that antiplane rupture (mode 3) in a LVFZ with $\Delta v = 0.5$ and $W = 1$ (Figure 8b) has a similar behavior as in-plane rupture (mode 2): an initial crack stops after spawning a pulse. In this case the pulse propagates at almost the S wave speed of the LVFZ, and its rise time ($\sim$0.3) is comparable to the travel time of SH waves inside the LVFZ. This proves that the generation of slip pulse does not necessarily require the conversion between P and S waves.

3.7. Effect of Frictional Healing

[18] The rate of fault strength recovery immediately after slip arrest, over time scales shorter than the rupture duration, still lacks constraints from observations and laboratory experiments. In our previous simulations we considered the end-member model of instantaneous healing, in which the friction coefficient recovers to its static value immediately after slip arrest. We consider now the opposite end-member model, in which frictional healing is absent (or extremely slow at coseismic time scales). Assuming that the friction coefficient remains at its dynamic level even after slip arrest, we found that the rupture in a LVFZ with $\Delta v = 0.4$ and $W = 1$ (Figure 9a) propagates as a pulse followed by multiple cracks with much lower slip rates. The rupture speed experiences a transition from the LVFZ Rayleigh to the country Rayleigh speed.

[19] Interestingly, this example features negative slip rates, i.e., in the direction opposite to the main slip direction. Indeed, the reflected waves can drop the fault shear stress to negative values, and, if the fault does not heal instantaneously, the stress can reach the dynamic strength again but with opposite sign. The fault can then slip backward until the stress rises up again once the reflected waves are past. The low dynamic friction coefficient assumed here (0.1) is consistent with the absence of large frictional heat produced by narrow principal slip zones in many natural faults [e.g., *Kanamori and Heaton*, 2000; *Boullier et al.*, 2001; *Kano et al.*, 2006]. However, the possibility of wide slip zones and high dynamic friction cannot be excluded. In a simulation with dynamic friction of 0.3, keeping the same stress drop and strength drop as previously, the negative shear stress is no longer large enough to reach the dynamic strength (Figure 9b). Thus, the fault does not slip backward if the dynamic fault strength is high enough. Overall, these two simulations with low and high friction yield very similar ruptures. The reverse slip rate remains a small-scale feature. Given the resolution limitations of current seismic source inversions, obtaining seismological evidence of reverse slip rates in natural earthquakes is challenging.

4. Discussion

4.1. Correlation Between LVFZ and Short Rise Time

[20] Source inversion studies inferred very short rise times ($\sim$0.3 s) from the strong motion data of the Morgan Hill earthquake [*Hartzell and Heaton*, 1986; *Beroza and Spudich*, 1988]. According to the relation (rise time) = (seismogenic thickness) ÷ (2 × rupture speed) proposed by *Day* [1982a], *Beroza and Spudich* [1988] found the short rise time implied a seismogenic thickness of 1 km, an unreasonably low value. *Cormier and Spudich* [1984] modeled a wedge-shaped low-velocity zone of 1–2 km wide in the Calaveras fault, which may have contributed to the short rise time of the 1984 Morgan Hill earthquake. *Spudich and Olsen* [2001] also

pointed out that a 30–100 m wide damage zone is possibly embedded in the 1–2 km wide low-velocity zone in Calaveras.

[21] We further analyze two earthquakes, 1992 Landers and 1999 Hector Mine, of which both LVFZ properties and rise time are well studied. Using techniques based on fault zone guided waves, the Landers LVFZ is 150–250 m wide [*Li et al.*, 1994], while other waveform techniques suggest a 270–360 m wide zone of 35%–60% velocity reduction [*Li et al.*, 2007]. The width of Hector Mine LVFZ inferred from guided wave studies is 75–100 m, and the S velocity is reduced by 40%–50% [*Li et al.*, 2002]. Our simulations suggest that narrower LVFZs like Hector Mine should lead to shorter rise times. *Ji et al.* [2002] compared the average rise time of the 1999 Hector Mine with that of 1992 Landers [*Wald and Heaton*, 1994] and found that they are similar to each other ($\sim$3.6 s for Hector Mine and $\sim$4 s for Landers). However, the initiation region of Hector Mine, which is probably well resolved, shows an average rise time of $\sim$1 s, much shorter than that of other regions. Limited by the seismic data and by other mechanisms that possibly contribute to short rise times, e.g., self-healing and bimaterial effects, we cannot conclude on a simple correlation between LVFZ properties and rise times. Thus, it is still significant for future study to enrich the database of fault zone properties and rise times and analyze the relative contributions of other pulse generation mechanisms.

4.2. Slip Pulses and Rupture Speed

[22] The shape of a slip pulse is strongly related to the rupture speed. For in-plane problems, the rupture speed could either approach the Rayleigh wave speed (subshear) or P wave speeds (supershear). In the presence of a LVFZ we found four rupture speed ranges: LVFZ Rayleigh, country Rayleigh, LVFZ supershear, and country supershear. Overall, LVFZ Rayleigh pulses have much shorter rise times and higher maximum slip rates than pulses with higher rupture speeds (compare Figure 4a with Figure 4b). Unlike the usual almost-singular shape at the rupture front, the country Rayleigh pulses for lower velocity reductions (Figures 4b and 7a) have a much smoother, almost sinusoidal shape. This suggests that the effect of a LVFZ on dynamic ruptures is a possible physical justification for the smooth slip rate time function assumed in some kinematic earthquake source inversions [*Ji et al.*, 2003]. Country Rayleigh pulses are dominant in narrow LVFZs ($W = 1$) with velocity reductions under 30% and for a wide range of initial stresses (Figures 6a and 6b). Given a shear modulus of 30 GPa and normal stress of 100 MPa, $W = 1$ corresponds to real LVFZ widths of a few 100 m for critical slip-weakening distances typical of large earthquakes (D_c of a several 10 cm). Hence, our results indicate that the LFVZ of mature faults might tend to smooth the slip rate during large earthquakes.

4.3. LVFZ Width and Rupture Style

[23] Usually the LVFZ has a width of 100–400 m, but some faults could accumulate a much thicker damage layer. *Savage and Brodsky* [2011] summarize fault zone properties from different studies and conclude that the total fault zone thickness is positively related to fault maturity, quantified by the accumulated fault displacement. The Calico fault is an exceptional example, which has a $\sim$1.5 km wide LVFZ. Our
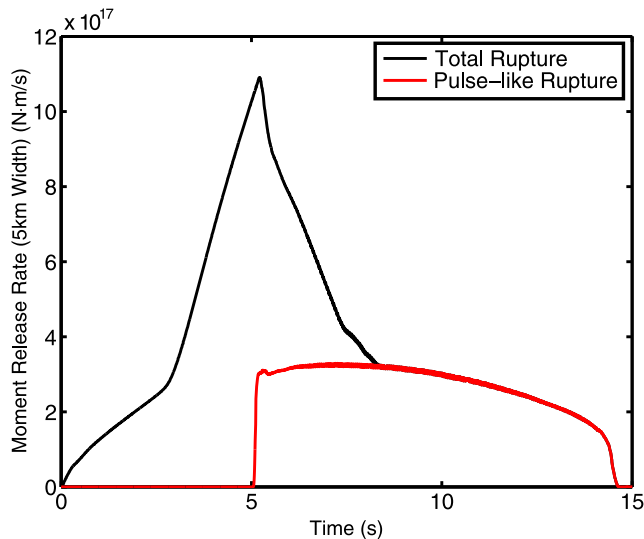
Figure 10. Moment release rate as a function of time for a 25 km long rupture inside a 600 m wide LVFZ with a velocity reduction of 40%. The red curve is the contribution from the pulse.

results show proportionality between LVFZ width and rise time. The crack-to-pulse transition also occurs later in wider LVFZs (Figures 5a and 5b). For $W = 4$ we found a complicated rupture pattern with coexisting cracks and pulses. Assuming scale dependency of the (apparent) slip-weakening distance D_c, our results suggest that this complexity might be present in large earthquakes (D_c of the order of 0.5 m) on wide LVFZs like the Calico fault zone, or in smaller events (D_c shorter than 10 cm) on LVFZs of the order of 100 m wide. For a given LVFZ width, our models predict a

decreasing degree of rupture complexity as a function of earthquake magnitude. Obviously, in natural faults the effects described here compete with other processes that contribute to rupture complexity.

4.4. Ground Motion

[24] LVFZs can trap waves [*Li et al.*, 1994] and amplify ground motions. *Spudich and Olsen* [2001] found a large 0.6–1.0 Hz frequency pulse at a station located 1.2 km away from the Calaveras LVFZ in the records of the 1984 M_w 6.2 Morgan Hill earthquake (source on the Calaveras fault) but not in the records of the 1989 M_w 6.9 Loma Prieta earthquake (source outside the Calaveras fault). They concluded that the large pulse is likely due to the amplification effect of the LVFZ.

[25] We examine here some effects of the LVFZ on dynamic rupture that might have observable implications on ground motions. We consider a rupture that runs for a distance of 25 km until stopped by a high-strength barrier. The density and S and P wave velocities are 2670 kg m^{-3}, 3464 m s^{-1} and 6000 m s^{-1}, respectively. We assume a 600 m wide LVFZ with a velocity reduction of 40%. The normal stress is 100 MPa, and the initial shear stress is 25 MPa. The rupture undergoes a crack-to-pulse transition at a distance of about 6 km and then propagates as a pure pulse. Assuming a 5 km wide seismogenic zone, we calculate the moment release rate generated by the whole rupture and by the contribution of the pulse (Figure 10). The crack-to-pulse transition generates a strong high-frequency phase. The pulse-like rupture exhibits a flattened distribution of moment release rate. Its contribution to the seismic moment is comparable to that of the initial crack. In some of our simulations a crack triggers multiple pulses at regular intervals (Figure 11a). Each of these pulse onsets radiates a strong high-frequency phase (Figure 11b). Their regular
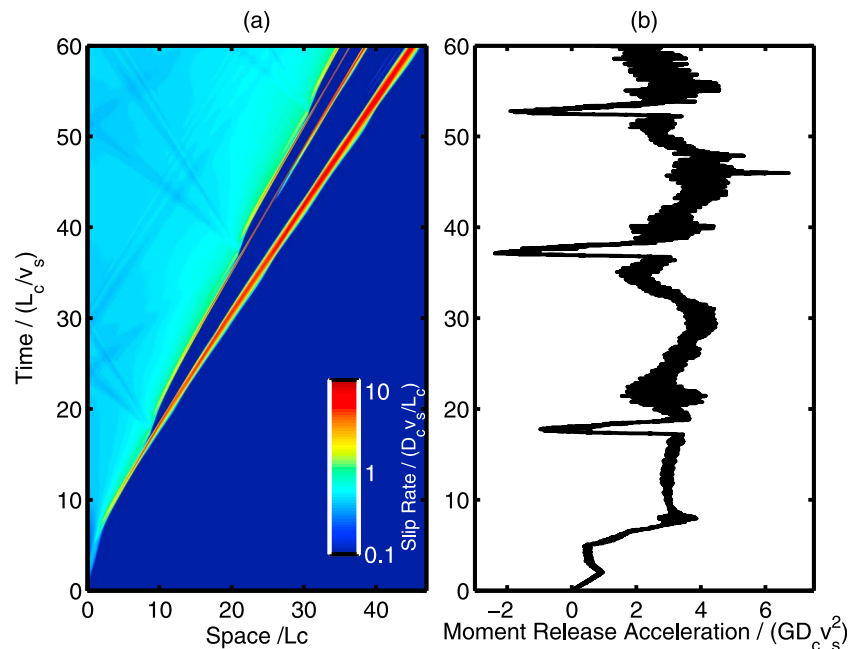

Figure 11. (a) Spatiotemporal distribution of slip rate and (b) moment release acceleration as a function of time for an S ratio of 1 and a LVFZ of width 1 with a velocity reduction of 20%.

sequence could contribute characteristic frequencies to the earthquake spectrum, although in less idealized situations this regularity might be broken by other complexities. Simulations by *Harris and Day* [1997, Figure 7] and *Ben-Zion and Huang* [2002, Figure 12] showed that multiple reflected waves in the LVFZ can generate oscillations of slip rate behind the rupture front. *Ben-Zion and Huang* [2002, appendix A] also discussed the effect of a single reflection on the rupture front. Our results reveal an effect of multiple reflections on the rupture front, which has a stronger signature on ground motions than the slip rate oscillations found by *Ben-Zion and Huang* [2002] and *Harris and Day* [1997]. Overall, our results show that the effect of LVFZ on dynamic rupture has a significant impact on the radiated wavefield.

5. Conclusions

[26] The earthquake source has a number of complexities, among which the existence of a LVFZ plays a significant role. It introduces multiple wave reflections that induce stress perturbations on the fault plane. We presented here dynamic rupture simulations on faults that bisect LVFZs of different velocity reductions and widths. We found that the LVFZ reflected waves can unload the fault and induce pulse-like ruptures (short rise times). The mechanism is most efficient when the time scale for frictional healing is sufficiently short. Our results show how the pulse shape, rise time, rupture speed, and complexity of the rupture process depend on the LVFZ properties. Pure pulse-like rupture is favored by high-velocity reduction and narrow width of the LVFZ. The rise time of slip pulses is proportional to the wave travel time across the LVFZ. The effect of the LVFZ can accelerate the transition to supershear rupture speed. Ruptures combining pulses and cracks are typical of LVFZs with lower-velocity reductions. These effects of the LVFZ on dynamic rupture have characteristic signatures on the radiated wavefield, contributing especially to high-frequency ground motions. Given the natural existence of LVFZ and the generality of the pulse generation mechanism presented here, it seems unlikely for earthquakes to propagate as pure cracks. However, a mixed crack-pulse rupture might not be distinguishable from a pure crack rupture at the low resolution of current seismological source observations.

Appendix A: Convergence Test in the Configuration of SCEC TPV3

[27] We first carry out a benchmark of SEM using the 2-D analog of the SCEC TPV3 problem [*Harris et al.*, 2009] and compare our results with those of another method, the DFM results of *Rojas et al.* [2008]. DFM is a highly efficient parallel finite difference code [*Day*, 1982b; *Harris and Day*, 1997; *Day and Ely*, 2002]. Both codes handle dynamic fault conditions based on the traction-at-split-node method [*Andrews*, 1999]. We model an isotropic, homogeneous, and elastic fault plane with density of 2670 kg m^{-3}, an S wave velocity of 3464 m s^{-1}, and a P wave velocity of 6000 m s^{-1}. The rupture is nucleated in a middle patch of 3000 m size and propagates for a distance of 15 km. The static friction is 0.677 and dynamic friction is 0.525 in the 30 km central segment. Rupture is stopped by abrupt barriers with much higher friction coefficients.

[28] We use 5 GLL nodes per spectral element side in our simulation. The equivalent grid size is the average spacing of GLL nodes, a quarter of the SEM element size. Thus, the SEM simulation with an element size of 50 m (SEM50) has the same spatial resolution as the DFM reference with grid size of 12.5 m (DFM12.5). We tested the following SEM element sizes: 75, 100, 125, 150, 187.5, 250, 300, 375, and 750 m. The rupture time is defined as the first time when the slip rate at a given location exceeds 1 mm/s. We calculate the RMS rupture time difference of each simulation compared with SEM50 and express the results as a percentage of the mean rupture time of SEM50. The RMS rupture time differences as well as time steps are shown as a function of average grid spacing in Figure A1a, the same representation used by *Rojas et al.* [2008]. The SEM results converge at approximately the same rate as the DFM results. However, the log-log plot of RMS rupture time difference as a function of grid spacing has a significant curvature for both SEM and DFM. To explain this curvature, we first observe that the rupture time in our SEM simulations converges locally (at each fault point) as a function of grid spacing. Moreover, this local convergence appears smooth and monotonic. We hence postulate that the rupture time $t(i, h)$ at position i is asymptotically related to the exact rupture time $t(i, 0)$ by

$$t(i, h) \approx t(i, 0) + c(i) h^p, \qquad (A1)$$

where h is the average grid spacing, $c(i)$ is a problem-dependent constant, and p is the leading-order exponent. This implies that the RMS rupture time difference of the jth simulation relative to the kth simulation is

$$e_{jk} = q\left(h_j^p - h_k^p\right), \qquad (A2)$$

where

$$q = \sqrt{\frac{\sum_{i=1}^{n} (c(i))^2}{n}}.$$

Figure A1b shows, as a function of grid spacing, the RMS rupture time difference of each simulation relative to three different reference simulations, SEM37.5, SEM50, and SEM75. The relative errors (with the exception of the coarser one, SEM750) follow a linear trend of the form of equation (A2) with $p = 1$. A least squares regression indicates that $q = 0.168$, independently of the choice of reference simulation. Figure A1c shows the rupture time errors corrected for the influence of the reference simulation ($q h_k$) as a function of grid spacing.

Appendix B: Comparison of Results of LVFZ Simulations With Those of DFM

[29] We ran a simulation of rupture in a LVFZ with SEM and DFM based on the same input parameters and compare the results as follows.

[30] We choose a 50 m grid size in DFM and a 200 m element size in SEM. The LVFZ that bisects the fault plane has a width of 800 m and a velocity reduction of 40% for both P and S waves. Specifically, the S wave speed of LVFZ is 2078.4 m s^{-1} and its P wave speed is 3600 m s^{-1}. The
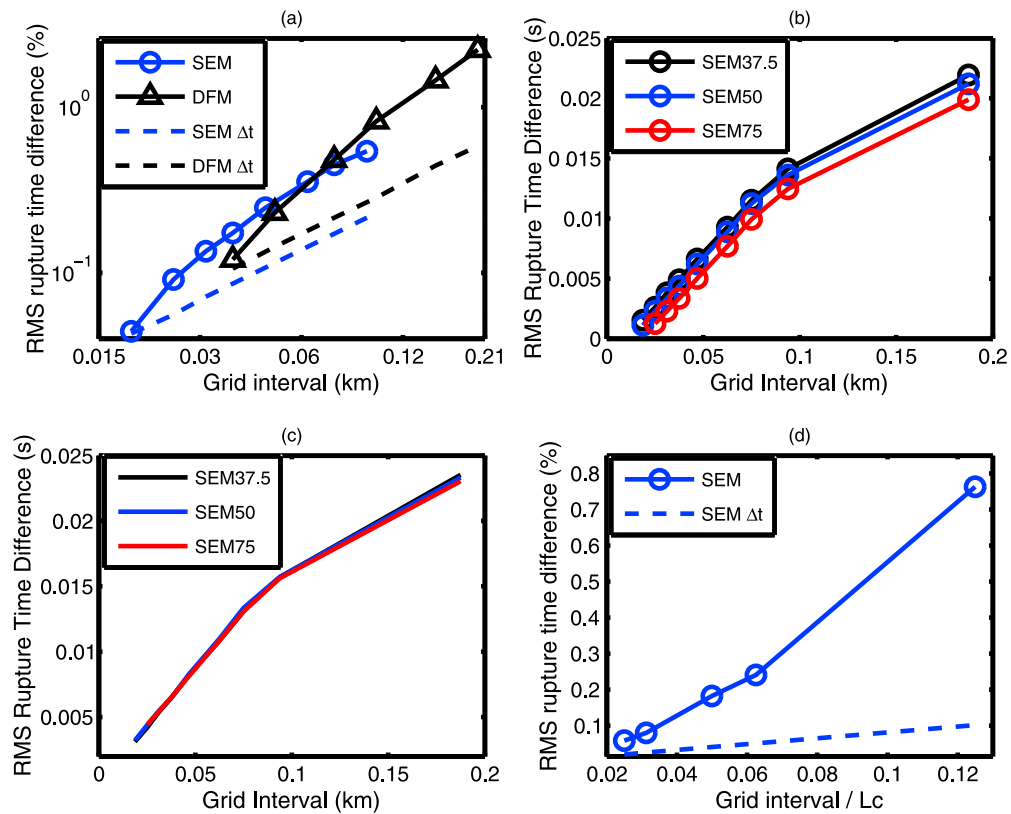
Figure A1. (a) RMS of rupture time difference relative to the finest-resolution simulation in the SCEC TPV3 problem as a function of grid interval for SEM and DFM (log-log scale). (b) Same as Figure A1a, but relative to SEM37.5, SEM50, and SEM75 (linear scale). (c) Same as Figure A1b after correcting for the effect of the reference simulation. (d) RMS rupture time difference relative to SEM0.0625 as a function of grid interval for SEM simulations in the LVFZ model setup.
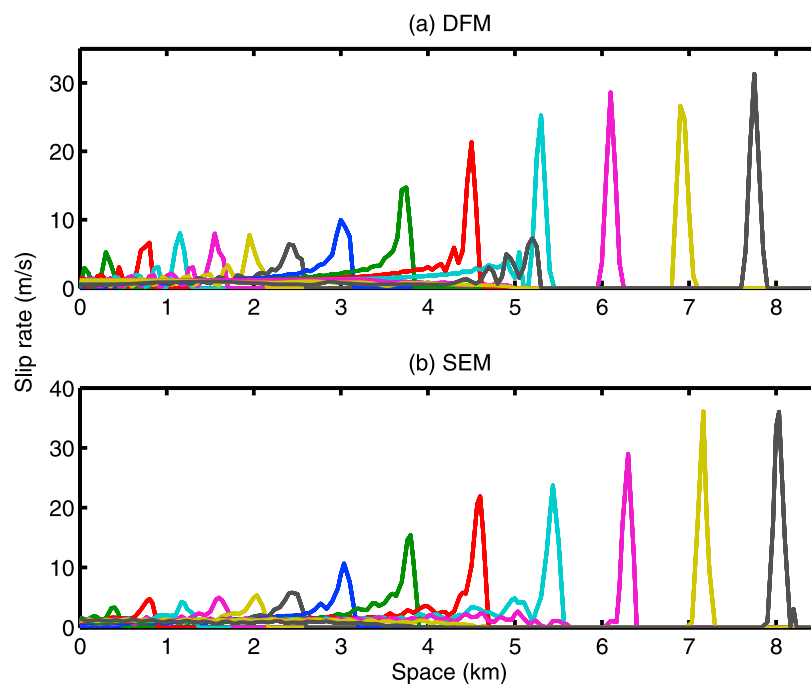

Figure B1. Spatial distributions of slip rate every 0.46 s for rupture inside an 800 m wide LVFZ with a velocity reduction of 40% computed with (a) DFM and (b) SEM.

friction law and coefficients are the same as described in section 2. The rupture propagates for 6.5 s total, during which the multiple reflected waves from the interface of LVFZ and country rock continuously alter the shear stress on the fault plane, resulting in slip rate oscillations and arrest episodes. Figures B1a and B1b show the spatial distribution of slip rate in a time interval of 0.46 s for both simulations.

[31] Slip pulses are generated in both SEM and DFM simulations. The rise times are short compared with the total rupture time. The slip rates at different times in both simulations are comparable, except inside the nucleation zone. The ruptures propagate at a relatively constant speed of about 1900 m s^{-1} after 4 s, which is the Rayleigh wave speed of the LVFZ. Overall, the two codes produce very similar patterns of slip functions and rupture processes.

[32] However, owing to the inherent differences between equivalent SEM and DFM simulations, we still see some minor differences, such as more high-frequency oscillations and a bit higher maximum slip rate in SEM. Since the GLL nodes are not evenly distributed, the required time step in SEM is always smaller than DFM, given the same equivalent grid size. Because the artificial viscosity on the fault plane is normalized by the actual time step in both codes, the SEM simulations are always less damped than their corresponding DFM simulation.

Appendix C: Convergence Test of the Dimensionless LVFZ Problem

[33] We show here that the simulations conserve numerical convergence in our LVFZ model setup using dimensionless quantities. We consider a LVFZ with $W = 2$ and $\Delta v = 0.4$. The onset of spontaneous rupture occurs around $t = 14$ and the simulation runs until $t = 45$. It is expected that as the ratio of element size to W decreases, the rupture process should be better resolved. In our simulation of finest resolution, SEM0.0625, the rupture behaves as a single pulse. Its healing phase is clean, the slip rate has weak high-frequency oscillations, and its peak amplitude grows gradually with time. Coarse simulations like SEM0.25 have instead a crack following the pulse. Figure A1d shows the RMS of the rupture time difference with respect to SEM0.0625, as a function of average grid size, including time steps for comparison. The simulations with finer resolution than SEM0.5 converge linearly, as found previously in our convergence tests in homogeneous media.

References

Aagaard, B. T., and T. H. Heaton (2008), Constraining fault constitutive behavior with slip and stress heterogeneity, *J. Geophys. Res.*, *113*, B04301, doi:10.1029/2006JB004793.

Aki, K., and P. G. Richards (2002), *Quantitative Seismology*, Univ. Sci. Books, Sausalito, Calif.

Ampuero, J. P., and Y. Ben-Zion (2008), Cracks, pulses and macroscopic asymmetry of dynamic rupture on a bimaterial interface with velocity weakening friction, *Geophys. J. Int.*, *173*(2), 674–692, doi:10.1111/j.1365-246X.2008.03736.x.

Ampuero, J. P., J. P. Vilotte, and F. Sanchez-Sesma (2002), Nucleation of rupture under slip dependent friction law: Simple models of fault zone, *J. Geophys. Res.*, *107*(B12), 2324, doi:10.1029/2001JB000452.

Andrews, D. J. (1976), Rupture velocity of plane strain shear cracks, *J. Geophys. Res.*, *81*(32), 5679–5687, doi:10.1029/JB081i032p05679.

Andrews, D. J. (1985), Dynamic plane-strain shear rupture with a slip-weakening friction law calculated by a boundary integral method, *Bull. Seismol. Soc. Am.*, *75*(1), 1–21.

Andrews, D. J. (1999), Test of two methods for faulting in finite-difference calculations, *Bull. Seismol. Soc. Am.*, *89*(4), 931–937.

Andrews, D. J., and Y. Ben-Zion (1997), Wrinkle-like slip pulse on a fault between different materials, *J. Geophys. Res.*, *102*(B1), 553–571, doi:10.1029/96JB02856.

Beeler, N., and T. Tullis (1996), Self-healing slip pulses in dynamic rupture models due to velocity-dependent strength, *Bull. Seismol. Soc. Am.*, *86*(4), 1130–1148.

Ben-Zion, Y., and Y. Huang (2002), Dynamic rupture on an interface between a compliant fault zone layer and a stiffer surrounding solid, *J. Geophys. Res.*, *107*(B2), 2042, doi:10.1029/2001JB000254.

Ben-Zion, Y., Z. Peng, D. Okaya, L. Seeber, J. G. Armbruster, N. Ozer, A. J. Michael, S. Baris, and M. Aktar (2003), A shallow fault-zone structure illuminated by trapped waves in the Karadere-Duzce branch of the North Anatolian Fault, western Turkey, *Geophys. J. Int.*, *152*(3), 699–717, doi:10.1046/j.1365-246X.2003.01870.x.

Beroza, G. C., and T. Mikumo (1996), Short slip duration in dynamic rupture in the presence of heterogeneous fault properties, *J. Geophys. Res.*, *101*(B10), 22,449–22,460, doi:10.1029/96JB02291.

Beroza, G. C., and P. Spudich (1988), Linearized inversion for fault rupture behavior: Application to the 1984 Morgan Hill, California, earthquake, *J. Geophys. Res.*, *93*(B6), 6275–6296, doi:10.1029/JB093iB06p06275.

Biegel, R. L., C. G. Sammis, and A. J. Rosakis (2008), An experimental study of the effect of off-fault damage on the velocity of a slip pulse, *J. Geophys. Res.*, *113*, B04302, doi:10.1029/2007JB005234.

Boullier, A. M., T. Ohtani, K. Fujimoto, H. Ito, and M. Dubois (2001), Fluid inclusions in pseudotachylytes from the Nojima fault, Japan, *J. Geophys. Res.*, *106*(B10), 21,965–21,977, doi:10.1029/2000JB000043.

Brietzke, G. B., and Y. Ben-Zion (2006), Examining tendencies of in-plane rupture to migrate to material interfaces, *Geophys. J. Int.*, *167*(2), 807–819, doi:10.1111/j.1365-246X.2006.03137.x.

Broberg, K. B. (1999), *Cracks and Fracture*, Academic, San Diego, Calif.

Cochard, A., and J. R. Rice (2000), Fault rupture between dissimilar materials: Ill-posedness, regularization, and slip-pulse response, *J. Geophys. Res.*, *105*(25), 891–907, doi:10.1029/2000JB900230.

Cochran, E. S., Y. G. Li, P. M. Shearer, S. Barbot, Y. Fialko, and J. E. Vidale (2009), Seismic and geodetic evidence for extensive, long-lived fault damage zones, *Geology*, *37*(4), 315–318, doi:10.1130/G25306A.1.

Cormier, V., and P. Spudich (1984), Amplification of ground motion and waveform complexity in fault zones: Examples from the San Andreas and Calaveras fault zones, *Geophys. J. R. Astron. Soc.*, *79*, 135–152.

Das, S., and K. Aki (1977), A numerical study of two dimensional spontaneous rupture propagation, *Geophys. J. R. Astron. Soc.*, *50*, 643–668.

Day, S. M. (1982a), Three-dimensional finite difference simulation of fault dynamics: Rectangular faults with fixed rupture velocity, *Bull. Seismol. Soc. Am.*, *72*(3), 705–727.

Day, S. M. (1982b), Three-dimensional simulation of spontaneous rupture: The effect of nonuniform prestress, *Bull. Seismol. Soc. Am.*, *72*(6), 1881–1902.

Day, S. M., and G. P. Ely (2002), Effect of a shallow weak zone on fault rupture: Numerical simulation of scale-model experiments, *Bull. Seismol. Soc. Am.*, *92*(8), 3022–3041, doi:10.1785/0120010273.

Harris, R. A., and S. M. Day (1997), Effects of a low-velocity zone on a dynamic rupture, *Bull. Seismol. Soc. Am.*, *87*(5), 1267–1280.

Harris, R. A., M. Barall, R. Archuleta, E. Dunham, B. Aagaard, J. Ampuero, H. Bhat, V. Cruz-Atienza, L. Dalguer, and P. Dawson (2009), The SCEC/USGS dynamic earthquake rupture code verification exercise, *Seismol. Res. Lett.*, *80*(1), 119–126, doi:10.1785/gssrl.80.1.119.

Hartzell, S. H., and T. H. Heaton (1986), Rupture history of the 1984 Morgan Hill, California, earthquake from the inversion of strong motion records, *Bull. Seismol. Soc. Am.*, *76*(3), 649–674.

Heaton, T. H. (1990), Evidence for and implications of self-healing pulses of slip in earthquake rupture, *Phys. Earth Planet. Inter.*, *64*(1), 1–20, doi:10.1016/0031-9201(90)90002-F.

Hickman, S. H., M. D. Zoback, and W. L. Ellsworth (2005), Structure and composition of the San Andreas fault zone at Parkfield: Initial results from SAFOD phase 1 and 2, *Eos Trans. AGU*, *86*(52), Fall Meet. Suppl., Abstract T23E-05.

Ji, C., D. J. Wald, and D. V. Helmberger (2002), Source description of the 1999 Hector Mine, California, earthquake, part II: Complexity of slip history, *Bull. Seismol. Soc. Am.*, *92*(4), 1208–1226, doi:10.1785/0120000917.

Ji, C., D. V. Helmberger, D. J. Wald, and K. F. Ma (2003), Slip history and dynamic implications of the 1999 Chi-Chi, Taiwan, earthquake, *J. Geophys. Res.*, *108*(B9), 2412, doi:10.1029/2002JB001764.

Kanamori, H., and T. H. Heaton (2000), Microscopic and macroscopic physics of earthquakes, in *Geocomplexity and the Physics of Earthquakes*, *Geophys. Monogr. Ser.*, vol. 120, edited by J. B. Rundle, D. L. Turcotte, and W. Klein, pp. 147–163, AGU, Washington, D. C., doi:10.1029/GM120p0147.

Kaneko, Y., J. P. Ampuero, and N. Lapusta (2011), Spectral-element simulations of long-term fault slip: Effects of low-rigidity layers on earthquake-cycle dynamics, *J. Geophys. Res.*, *116*, B10313, doi:10.1029/2011JB008395.

Kano, Y., J. Mori, R. Fujio, H. Ito, T. Yanagidani, S. Nakao, and K. F. Ma (2006), Heat signature on the Chelungpu fault associated with the 1999 Chi-Chi, Taiwan earthquake, *Geophys. Res. Lett.*, *33*, L14306, doi:10.1029/2006GL026733.

Lewis, M. A., and Y. Ben-Zion (2010), Diversity of fault zone damage and trapping structures in the Parkfield section of the San Andreas Fault from comprehensive analysis of near fault seismograms, *Geophys. J. Int.*, *183*(3), 1579–1595, doi:10.1111/j.1365-246X.2010.04816.x.

Lewis, M. A., Z. Peng, Y. Ben-Zion, and F. L. Vernon (2005), Shallow seismic trapping structure in the San Jacinto fault zone near Anza, California, *Geophys. J. Int.*, *162*(3), 867–881, doi:10.1111/j.1365-246X.2005.02684.x.

Li, H., L. Zhu, and H. Yang (2007), High resolution structures of the Landers fault zone inferred from aftershock waveform data, *Geophys. J. Int.*, *171*(3), 1295–1307, doi:10.1111/j.1365-246X.2007.03608.x.

Li, Y. G., and P. Leary (1990), Fault zone trapped seismic waves, *Bull. Seismol. Soc. Am.*, *80*(5), 1245–1271.

Li, Y. G., K. Aki, D. Adams, A. Hasemi, and W. H. K. Lee (1994), Seismic guided waves trapped in the fault zone of the Landers, California, earthquake of 1992, *J. Geophys. Res.*, *99*(B6), 11,705–11,722, doi:10.1029/94JB00464.

Li, Y. G., J. E. Vidale, S. M. Day, and D. D. Oglesby (2002), Study of the 1999 M 7.1 Hector Mine, California, earthquake fault plane by trapped waves, *Bull. Seismol. Soc. Am.*, *92*(4), 1318–1332, doi:10.1785/0120000909.

Li, Y. G., P. Chen, E. S. Cochran, J. E. Vidale, and T. Burdette (2006), Seismic evidence for rock damage and healing on the San Andreas fault associated with the 2004 M 6.0 Parkfield earthquake, *Bull. Seismol. Soc. Am.*, *96*(4B), S349–S363, doi:10.1785/0120050803.

Mizuno, T., Y. Kuwahara, H. Ito, and K. Nishigami (2008), Spatial variations in fault-zone structure along the Nojima fault, central Japan, as inferred from borehole observations of fault-zone trapped waves, *Bull. Seismol. Soc. Am.*, *98*(2), 558–570, doi:10.1785/0120060247.

Oglesby, D. D., and S. M. Day (2002), Stochastic fault stress: Implications for fault dynamics and ground motion, *Bull. Seismol. Soc. Am.*, *92*(8), 3006–3021, doi:10.1785/0120010249.

Peng, Z., Y. Ben-Zion, A. J. Michael, and L. Zhu (2003), Quantitative analysis of seismic fault zone waves in the rupture zone of the 1992 Landers, California, earthquake: Evidence for a shallow trapping structure, *Geophys. J. Int.*, *155*(3), 1021–1041, doi:10.1111/j.1365-246X.2003.02109.x.

Perrin, G., J. R. Rice, and G. Zheng (1995), Self-healing slip pulse on a frictional surface, *J. Mech. Phys. Solids*, *43*(9), 1461–1495, doi:10.1016/0022-5096(95)00036-I.

Rojas, O., S. Day, J. Castillo, and L. A. Dalguer (2008), Modelling of rupture propagation using high-order mimetic finite differences, *Geophys. J. Int.*, *172*(2), 631–650, doi:10.1111/j.1365-246X.2007.03651.x.

Rubin, A. M., and J. P. Ampuero (2007), Aftershock asymmetry on a bimaterial interface, *J. Geophys. Res.*, *112*, B05307, doi:10.1029/2006JB004337.

Savage, H. M., and E. E. Brodsky (2011), Collateral damage: Evolution with displacement of fracture distribution and secondary fault strands in fault damage zones, *J. Geophys. Res.*, *116*, B03405, doi:10.1029/2010JB007665.

Shi, Z., and Y. Ben Zion (2006), Dynamic rupture on a bimaterial interface governed by slip weakening friction, *Geophys. J. Int.*, *165*(2), 469–484, doi:10.1111/j.1365-246X.2006.02853.x.

Spudich, P., and K. Olsen (2001), Fault zone amplified waves as a possible seismic hazard along the Calaveras fault in central California, *Geophys. Res. Lett.*, *28*(13), 2533–2536, doi:10.1029/2000GL011902.

Wald, D. J., and T. H. Heaton (1994), Spatial and temporal distribution of slip for the 1992 Landers, California, earthquake, *Bull. Seismol. Soc. Am.*, *84*(3), 668–691.

Yang, H., and L. Zhu (2010), Shallow low-velocity zone of the San Jacinto fault from local earthquake waveform modeling, *Geophys. J. Int.*, *183*(1), 421–432, doi:10.1111/j.1365-246X.2010.04744.x.

Yang, H., L. Zhu, and E. S. Cochran (2011), Seismic structures of the Calico fault zone inferred from local earthquake travel time modeling, *Geophys. J. Int.*, *186*(2), 760–770, doi:10.1111/j.1365-246X.2011.05055.x.

Zheng, G., and J. R. Rice (1998), Conditions under which velocity-weakening friction allows a self-healing versus a cracklike mode of rupture, *Bull. Seismol. Soc. Am.*, *88*(6), 1466–1483.

J.-P. Ampuero and Y. Huang, Division of Geological and Planetary Sciences, California Institute of Technology, 1200 E. California Blvd., MS 252-21, Pasadena, CA 91125, USA. (ampuero@gps.caltech.edu; yhuang2@caltech.edu)